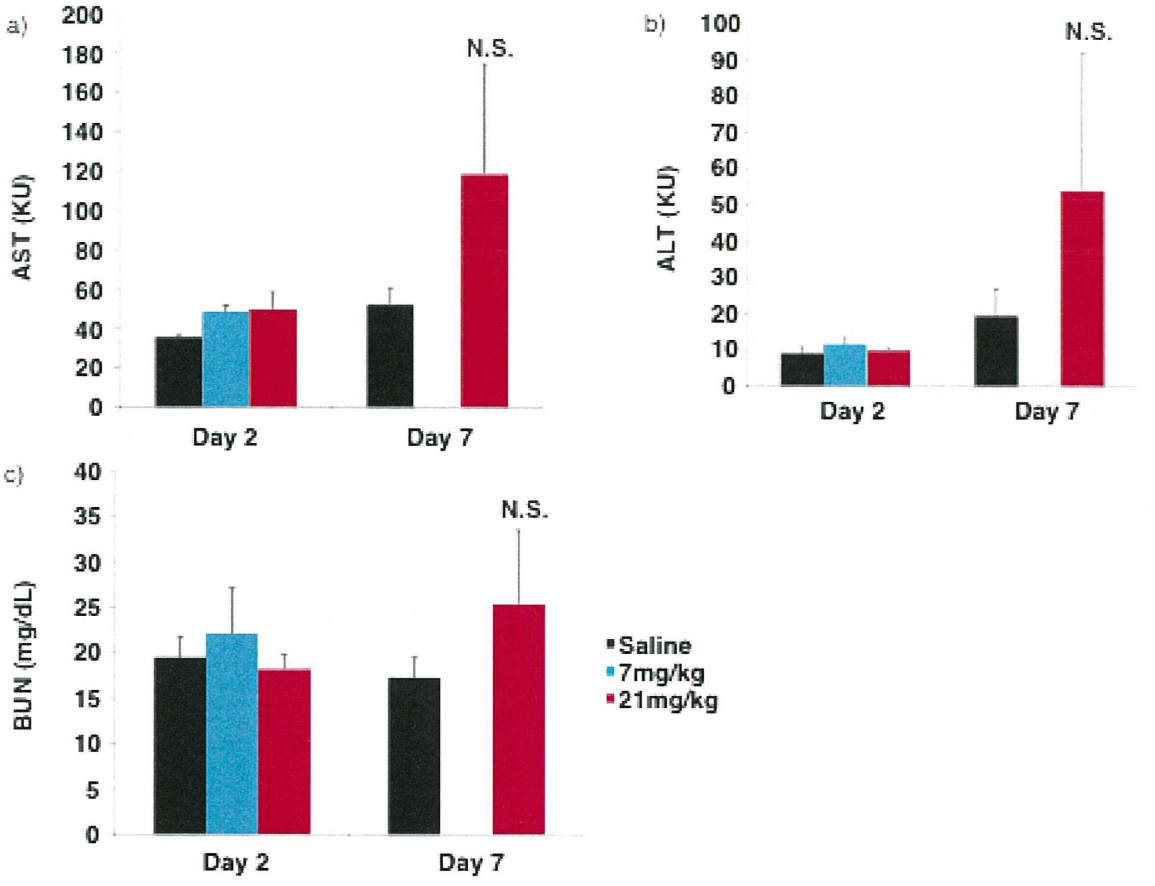

図 8 Changes in toxicological parameters upon A346SL13 dosing. (a), (b) and (c) Serum liver transaminases (AST and ALT) and BUN levels were measured. Data represent mean values ± SD. N.S. means not significant.

厚生労働科学研究費補助金　（創薬基盤推進研究事業）
分担研究報告

ApoC-Ⅲをターゲットとした革新的核酸医薬の有効性及び安全性評価

分担研究者　柴田　雅朗　大阪保健医療大学・教授

研究要旨

本研究は、アンチセンス医薬の有効性・安全性について病理組織学的に評価し、さらに有効で安全なApoC-Ⅲに対するBNA搭載アンチセンス医薬の開発に資する情報の提供を目的としている。今回、*in vitro*スクリーニングで選択されたBNA搭載アンチセンス分子がマウスの肝臓内の脂肪沈着の減少を促進することを見出し、*in vitro*スクリーニングの有効性が示された。一方で、軽微な毒性の発現を確認した。有効性及び安全性を兼ね備えたBNA搭載アンチセンス分子を見つけ出すためには、*in vivo*スクリーニングの強化が重要であることが示唆された。また、副作用の低減を狙って、分子設計を見直すことも有効であると考えられる。

A.　研究目的

アンチセンス医薬などの新型医薬品を臨床応用するためには、アンチセンス医薬の有効性及び安全性に関する情報を可能な限り広く収集することが必要である。本研究では、ApoC-Ⅲに対する BNA 搭載アンチセンス医薬の有効性・毒性・安全性について病理組織学的に評価し、多角的な情報を提供することを目的としている。また、さらに有効で安全な ApoC-Ⅲに対する BNA 搭載アンチセンス医薬の開発に資する情報を提供する。

B. 研究方法

1. 高トリグリセリド（TG）血症モデルマウスの作成

高 TG 血症マウスを作成するために高脂肪、高ショ糖、高カロリーを特徴とした特別食（F2WTD, オリエンタル酵母工業）を利用した。

2. アンチセンスオリゴヌクレオチドの調製

2',4'-BNA/LNAの人工核酸で部分的に修飾されたホスホロチオアート型のアンチセンスを設計した（表１）。2',4'-BNA^{NC}のアミダイトユニットは株式会社BNAから購入した。2',4'-BNA/LNAあるいは2',4'-BNA^{NC}を搭載したホスホロチオアート型オリゴヌクレオチドは株式会社ジーンデザインより購入した。オリゴヌクレオチドの合成は一

般的なホスホロアミダイト法により行われ、生成物は無菌条件下で注意深く取り扱われ精製された。全ての製品はエンドトキシンフリーや低残塩量が保証されており、*in vivo* での使用に適した状態で提供されている。

3. 反復投与試験

被験動物として 6 週齢の雄マウス C57BL/6J（日本クレア）を各投与群で例数 5 匹となるように準備した。3 週間の高脂肪食 F2WTD（オリエンタル酵母工業株式会社）負荷の後、アンチセンスを 1 週間で 2 回全 5 回、腹腔内投与を行った。3 回目及び 5 回目の投与翌日に尾静脈より絶食下採血を行なった。16 日目にマウスを麻酔後、PBS で下大静脈より灌流した。

4. 単回投与実験

被験動物として6週齢のマウスC57BL/6J（♂:日本クレア）を各投与群で例数5匹となるように準備した。負荷の後、0日目に採血して、アンチセンスを静脈内より単回投与した（0, 7, 21 mg/kg）。投与後2及び7日目に絶食下尾静脈より採血し、ジエチルエーテルで麻酔後、PBSで下大静脈より灌流し、肝臓を採取した。

5. 病理組織学的解析

肝臓を採取して、20%ホルマリン緩衝液に24時間浸して固定した後6時間流水水洗し、パラフィン包埋した。ミクロトーム（Leica Microsystems）を用いて薄切切片（5μm）を作製して、Carrazzi's hematoxylin 及び Tissue-Tek eosinを用いてヘマトキシシリン・エオジン染色を行ない、顕微鏡にて観察し、写真撮影した。

C. 研究結果

1. 2',4'-BNA/LNA搭載抗ApoC-Ⅲアンチセンス**A3495SL20**の安全性評価

BNA 搭載抗 ApoC-Ⅲアンチセンス（**A3495S20**、**A3495SL20**）が高脂血症マウスで薬効を示し得るかどうかを検討するために、6 週齢の C57BL/6J の雄マウスに対して 2 週間高脂肪食負荷を行い、その後週 2 回の頻度で計 5 回、腹腔内より 20 mg/kg/injection の投与量でアンチセンスの反復投与を行った。実験終了時まで高脂肪食の給餌を継続した。試験群は全 3 群で、生理食塩水投与群、**A3495S20**（従来のアンチセンス）投与群、**A3495SL20**（BNA 搭載アンチセンス）投与群とし、例数は各群 5 匹とした。採血は絶食下に投与前と 3 回目投与後と最終 5 回目投与後の計 3 回行った。初回投与から 16 日後にマウスを屠殺し、全血の採血及び肝臓の摘出を行った。投与前後で群間に体重の差は認められず、摂食や摂水障害なども観察されなかった。

他方、**A3495SL20** の投与量依存性について検討するために 6 週齢の C57BL/6J の雄マウスに対して 2 週間高脂肪食（F2WTD）負荷を行い、その後、週 2 回の頻度で計 5 回、腹腔内より 1、5、10 mg/kg/injection の投与量で **A3495SL20** の反復投与を行った。実験終了時まで高脂肪食の給餌は継続した。試験群は生理食塩水投与群及び

A3495SL20 投与群（3 群）の計 4 群、例数は各群 5 匹とした。採血は絶食下に投与前と 3 回目投与後と最終 5 回目投与後の計 3 回行った。初回投与から 16 日後にマウスを屠殺し、全血の採血、肝臓の摘出を行った。本実験におけるマウスの各個体における肝臓の病理組織学的な解析を行った。生理食塩水投与群の全例で門脈周辺域における肝細胞の脂肪変性が認められたが、1 mg/kg 以上の投与群で脂肪変性は観察されなかった（図 1、表 2）。これはアンチセンス投与群にみられた血清脂質の低下と一致する。一方、20 mg/kg 群で肝細胞の顆粒状変性が全例に観察され、投与に起因する所見と考えられた。また、1 mg/kg 以上の投与各群で 1 ないし 2 例の肉芽腫が認められたが、用量依存性がないことから、投与に起因する所見とは考え難かった。腎臓では目立った病理組織学的所見は認められなかった（**表 2**）。

これらの所見から **A3495SL20** には肝細胞の脂肪変性を抑制する作用のあることが示唆されたが、20 mg/kg の高用量群では肝細胞の変性所見を呈し、毒性変化をもたらした。

2. **A346SL13**の*in vivo*薬効評価

A346SL13は分子内に2',4'-BNA/LNA修飾を有し、鎖長は13 merである。**A346SL13**の安全性を評価するために、6週齢のC57BL/6Jの雄マウスに対して2週間高脂肪食（F2WTD）負荷を行い、その後、**A346SL13**を尾静脈より7及び21 mg/kgの投与量で単回投与を行った。血液生化学検査によれば7日目において21mg/kg投与群に毒性の兆候が見出され（図2）、病理組織学的解析においても21 mg/kg投与群では、軽度の白血球浸潤が観察され（表3、図3）、血液生化学的データと関連している所見と考えられた。

D. 考察

ApoC-Ⅲに対するアンチセンスの投与に伴う、肝細胞における脂肪変性の減少が認められた。このことは、斯波らのグループによって見出された治療効果としての血清中のトリグリセリドの大幅な減少と一致する。一方で、投与量の増加に伴って軽微な細胞浸潤や顆粒変性といった毒性変化が認められた。これらの毒性については、①標的分子の抑制に起因する毒性か②化合物に起因する毒性が考えられる。①ApoC-Ⅲの阻害に起因する毒性の可能性については、ApoC-Ⅲの機能欠損患者が健康でかつ動脈硬化のリスクが低いことやノックアウトマウスが致死性でないことから類推すれば可能性は低いと考えられる。他方でアンチセンス薬剤の場合、②の化合物に起因する毒性はさらにA)配列に起因する毒性とB)特定の化学構造に起因する毒性に大別できる。配列によっては内在の免疫システムを活性化するものや標的以外と結合し、予期せぬ効果を引き起こすものもある。特定の化学構造とは例えばホスホロチオアート結合やBNAなどの化学構造のことを指す。ホスホロチオアートは、リン酸結合の非架橋の酸素のひとつを硫黄原子に置換した構造を有

し、化学的には酸素原子に比べると柔らかく、疎水性的な性質を有しており、タンパク質との非特異的な相互作用をしやすいと考えられている。ホスホロチオアートに起因する毒性についてはこれまでに多くの報告がある。また最近では2',4'-BNA/LNAに起因する毒性もいくつか報告されている。これらのことから本検討で観察された毒性の原因としては②の化合物に起因する毒性であることが推測され、特に20merから13merへの鎖長の短縮に伴い、2',4'-BNA/LNAの導入数は減少していることから、配列に起因する毒性であると推測できる。*In vitro*スクリーニングによって、脂質低下効果の極めて高いアンチセンス分子の選択が可能であることを見出したが、今回*in vivo*試験を実施した分子については毒性の発現が見出された。**A346SL13**の毒性惹起作用が何に起因するかについては現段階では推定し難いが、両者は鎖長及び2',4'-BNA/LNAの導入数は等しく、可能性としてはアンチセンスの短鎖化に伴う他の標的に結合する確率（off-target効果）が高まったことが考えられる。BLAST（Basic Local Alignment Tool）による解析によればマウスの遺伝子及び転写産物中に完全相補配列が**A346SL13**では約190存在するとされる。また20merの**A2495SL20**の場合においても完全マッチ遺伝子はApoC-Ⅲ遺伝子のみであるが、部分的に相補鎖形成が可能な遺伝子は数多く存在することになる。現時点では少なくともoff-targetの候補の数に関して言えば副作用を予測する重要な因子である可能性は考えられる。

本検討から、*in vitro*スクリーニングで選択された候補分子の中から、薬効の大きさに加えて低毒性なアンチセンス分子を選出するために*in vivo*スクリーニングを強化するする必要があると考えられる。また、off-target効果削減の意味では鎖の長さはある程度の鎖長を保ち、しかも部分マッチでは機能しないように特異性を上げる分子設計の工夫が有効ではないかと考えられる。

E. 結論

本研究では、病理組織学的な観察によって、2',4'-BNA/LNA搭載したアンチセンス（**A3495SL20、A346SL13**）が肝臓内脂肪沈着の減少作用を有することを見出した。一方で、投与量の増加に伴って軽微な細胞浸潤や顆粒変性といった毒性が認められた。今後、*in vivo*スクリーニングを強化することによって有効性及び安全性を兼ね備えたBNA搭載アンチセンス分子を見つけ出すことが可能となるだろう。また、off-target効果の削減等を狙って、分子設計を見直すことも有効であると考えられる。

F. 健康危険情報

本研究では現在のところ健康に危険を及ぼす可能性はない。

G. 研究発表

1. 論文発表

原著論文

1. Yamamoto T, Harada-Shiba M, Nakatani M, Wada S, Yasuhara H, Narukawa K, Sasaki K, Shibata M.A, Torigoe H, Yamaoka T, Imanishi T, Obika S: Cholesterol-Lowering Action of BNA-based Antisense Oligonucleotides Targeting PCSK9 in Atherogenic Diet-Induced Hypercholesterolemic Mice: Molecular Therapy Nucleic Acid, in press
2. Ito Y, Shibata M, Eid N, Morimoto J, and Otsuki Y, Lymphangiogenesis and axillary lymph node metastasis correlated with VEGF-C expression in two immunocompetent mouse mammary carcinoma models, Int. J. Breast Cancer, 2011, Electronic resource# 867152.
3. Shibata M.A, Iinuma M, Morimoto J, Kurose H, Akamatsu K., Okuno Y, Akao Y, and Otsuki Y, α-Manogstin extracted from the pericarp of the mangosteen (Garcinia mangostana Linn) reduces tumor growth and lymph node metastasis in an immunocompetent xenograft medel of metastatic mammary cancer carrying a p53 mutation. BMC Med., 9, Electronic resource# 69.2011.
4. Shibata M.A, Morimoto J, Shibata E, Harada-Shiba M, and Fujioka S, Inhibition of tumor growth and metastasis by a combination of anti-VEGF-C and enhanced IL-12 therapy in an immunocompetent mouse mammary cancer model. In Gunduz, E.G.a.M. (ed.), Breast Cancer - Current and Alternative Therapeutic Modalities. InTech, Rijieka, pp. 489-502,2011.

2. 学会発表

1. 柴田雅朗, Ambati Jayakrishna, Albuquerque Romulo, 森本純司, 伊藤裕子, 大槻勝紀：リンパ管新生を標的とした新規内因性 VEGF 受容体２型のマウス乳癌リンパ節転移抑制. 第 43 回日本臨床分子形態学会・学術集会 講演要旨集, 34 頁. 2011 年 9 月 9 日,大阪
2. 柴田雅朗, 森本純司, 伊藤裕子, 大槻勝紀： Splicing variant である新規可溶性 VEGF 受容体２型は高転移性マウス乳癌のリンパ節転移を抑制する. 第 116 回日本癌学会学術総会 Proceeding 176 頁. 2011 年 10 月 3 日, 名古屋
3. 柴田雅朗、Ambati Jayakrishna, Albuquerque Romulo, 森本純司: 新規内因性のリンパ管新生抑制因子である可溶性 VEGF 受容体２型のマウス乳癌に対するリンパ節転移抑制作用. 第 28 回日本毒性病理学会総会・学術集会講演要旨集, 86 頁. 2011 年 2 月 2 日,東京

H. 知的財産権の出願・登録状況

なし

表 1 Antisenses used in this study

	Sequence ID	Sequence
1	A3495S20	5′-tcttatccagctttattagg-3′
2	A3495SL20	5′-TCtTaTCcagcttTaTTaGg-3′
3	A346SL13	5'-CTGcatggcaCCT-3'

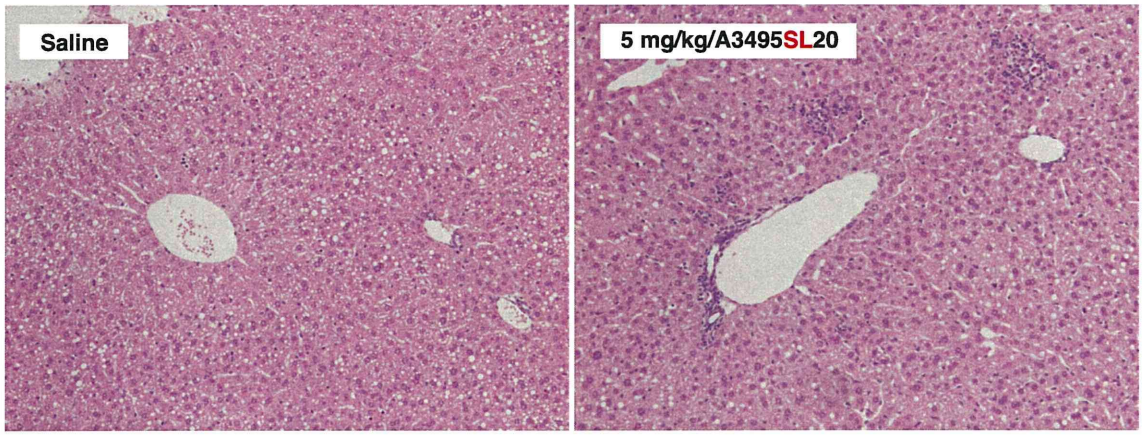

図 1 Representative H&E stein images of liver of saline- and 5 mg/kg of A3495SL20-treated mice.

表 2 Histopathological findings

			Control	A3495SL20				A3495S20
	DOSE (mg/kg) --		0	1	5	10	20	20
	NO. OF MICE EXAMINED --		4	5	5	5	5	5
Liver	Normal		0	3	3	3	0	2
	Not Examined		0	1	0	0	0	0
	Fatty change, periportal	+	4	0	0	0	0	0
	Granular degeneration, periportal	+	0	0	0	0	5	0
	Granuloma	+	0	1	2	1	1	2
Kidneys	Normal		4	4	5	5	5	4
	Hemorrhage		0	0	0	0	0	1

Grading: ±, trace; +, slight; ++, moderate.

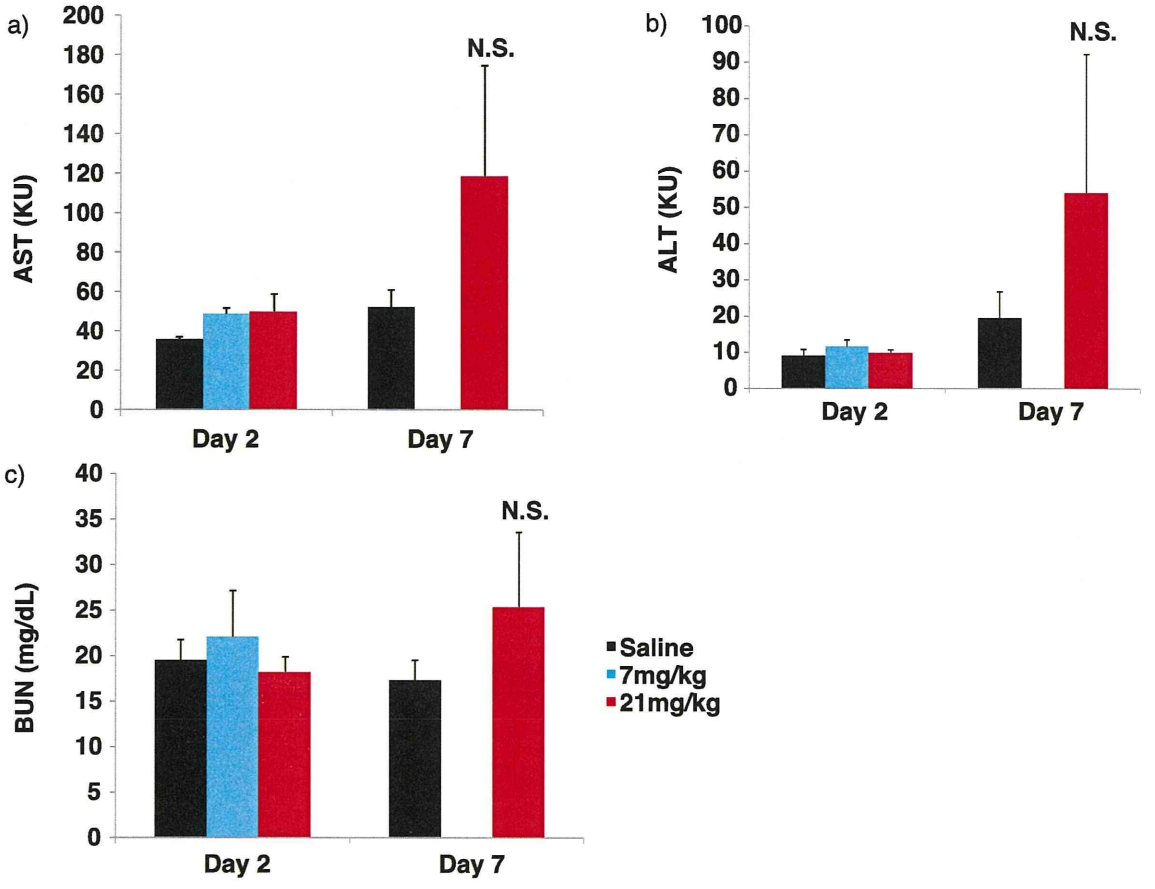

図 2 Changes in toxicological parameters upon A346SL13 dosing. (a), (b) and (c) Serum liver transaminases (AST and ALT) and BUN levels were measured. Data represent mean values ± SD. N.S. means not significant.

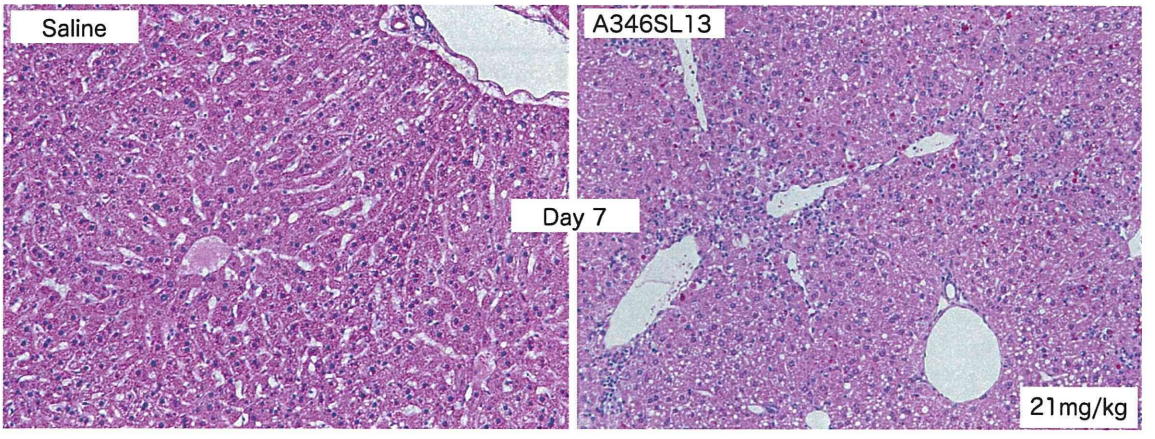

図 3 Representative H&E stein images of liver on day 2 and 7 of saline- and 7 and 21 mg/kg A346SL13- treated mice.

表 3 Histopathological findings

ORGAN AND FINDINGS			DAY 2		
	DOSE (mg/kg) --		0	7	21
	NO. OF ANIMALS EXAMINED --		3	3	3
Liver			(3)	(3)	(3)
	Cellular infiltration	+	0	1	0
	Granuloma	+	1	0	1
	Vacuolization (Vacuolation), cytoplasmic	±	1	0	1
		+	1	3	2
		++	1	0	0
Kidney(s)			(3)	(3)	(3)
	Normal		3	3	3

Grading: ±, trace; +, slight; ++, moderate.

			DAY 7	
	DOSE (mg/kg) --		0	21
	NO. OF ANIMALS EXAMINED --		3	3
Liver			(3)	(3)
	Normal		1	0
	Cellular infiltration	±	0	1
		+	0	2
	Granuloma	±	1	0
		++	1	0
	Vacuolization (Vacuolation), cytoplasmic	+	1	2
		++	1	0
Kidney(s)			(1)	(0)
	Cellular infiltration	+	1	0

Grading: ±, trace; +, slight; ++, moderate.

研究成果の刊行に関する一覧表

書籍

著者氏名	論文タイトル名	書籍全体の編集者名	書　籍　名	出版社名	出版地	出版年	ページ
Iwamoto N, Harada-Shiba M	Intratracheal Gene Transfer Using Polyplex Nanomicelles and Their Application to Cardiology, Nanomedicine and the Cardiovascular System	Victor R. Preedy	Nanomedicine and the Cardiovascular System	Science Publishers	New Hampshire,USA	2011年	284-302

雑誌

発表者氏名	論文タイトル名	発表誌名	巻号	ページ	出版年
Torigoe H, Nakagawa O, Imanishi T, Obika S, Saisaki K	Chemical Modification of Triplex-forming Oligonucleotide to Promote Pyrimidine Motif Triplex Formation at Physiological pH	Biochimie	94	1032-1040	2012年
Ito K. R, Kodama T, Makimura F, Hosoki N, Osaki T, Orita A, Imanishi T, Obika S	Cleavage of Oligonucleotides Containing a P3'→N5' Phosphoramidate Linkage Mediated by Single-stranded Oligonucleotide Templates	Molecules	16	10695-10708	2011年
Mori K, Kodama T, Obika S	Design, Synthesis and Properties of Boat-shaped Glucopyranosyl Nucleic Acid	Org. Lett	13	6050-6053	2011年
Shrestha A. R, Hari Y, Yahara A, Osawa T, Obika S	Synthesis and Properties of a Bridged Nucleic Acid with a Perhydro-1,2-oxazin-3-one Ring	J. Org. Chem	76	9891-9899	2011年
Morihiro K, Kodama T, Obika S	Benzylidene Acetal-Type Bridged Nucleic Acids: Changes in Properties Upon Cleavage of the Bridge Triggered by External Stimuli	Chem. Eur. J	17	7918-7926	2011年

Mori K, Kodama T, Baba T, Obika S	Bridged Nucleic Acid Conjugates at 6'-Thiol: Synthesis, Hybridization Properties and Nuclease Resistances	Org. Biomol. Chem	9	5272-5279	2011年
小比賀　聡	糖部架橋型核酸の医薬への応用	医薬ジャーナル	48	65-69	2012年
Yamamoto T, Harada-Shiba M, Nakatani M, Wada S, Yasuhara H, Narukawa K, Sasaki K, Shibata M.A, Torigoe H, Yamaoka T, Imanishi T, Obika S	Cholesterol-Lowering Action of BNA-based Antisense Oligonucleotides Targeting PCSK9 in Atherogenic Diet-Induced Hypercholesterolemic Mice	Molecular Therapy Nucleic Acid			in press
Sugisawa T, Okamura T, Makino H, Watanabe M, Kishimoto I, Miyamoto Y, Iwamoto N, Yamamoto A, Yokoyama S, Harada-Shiba M	Defining patients at extremely high risk for coronary artery disease in heterozygous familial hypercholesterolemia	Journal of Atherosclerosis and Thrombosis	19,4	369-375	2012年
Yokoyama S, Yamashita S, Ishibashi S, Sone H, Oikawa S, Shirai K, Ohta T, Bujo H, Kobayashi J, Arai H, Harada-Shiba M, Eto M, Hayashi T, Gotoda T, Suzuki H, Yamada N	Background to discuss guidelines for control of plasma HDL-cholesterol in Japan	ournal of Atherosclerosis and Thrombosis	19,3	207-212	2012年
Uchida S, Itaka K, Chen Q, Osada K, Miyata K, Ishii T, Harada-Shiba M, Kataoka K	Combination of chondroitin sulfate and polyplex micelles from Poly(ethylene glycol)-poly{N'-[N-(2-aminoethyl)-2-aminoethyl]aspartamide} block copolymer for prolonged in vivo gene transfection with reduced toxicity	J Control Release	155	296-302	2011年
斯波真理子	高LDLコレステロール血症	CURRENT THERAPY	30,3	33-38	2012年
斯波真理子	脂質異常症の病態と治療　家族性高コレステロール血症	臨牀と研究	88,10	45-49	2011年

斯波真理子	家族性高コレステロール血症の診断と治療	日本医師会雑誌	140,6	1247-1250	2011年
斯波真理子	家族性高コレステロール血症をどのように診るか?	Heart View	15,9	32-37	2011年
斯波真理子	家族性高コレステロール血症をどう扱うか	medicina	48,5	837-841	2011年
Ito Y, Shibata M, Eid N, Morimoto J, and Otsuki Y	Lymphangiogenesis and axillary lymph node metastasis correlated with VEGF-C expression in two immunocompetent mouse mammary carcinoma models	Int. J. Breast Cancer	Electronic resource# 867152		2011年
Shibata M.A, Iinuma M, Morimoto J, Kurose H, Akamatsu K., Okuno Y, Akao Y, and Otsuki Y	α-Manogstin extracted from the pericarp of the mangosteen (Garcinia mangostana Linn) reduces tumor growth and lymph node metastasis in an immunocompetent xenograft medel of metastatic mammary cancer carrying a p53 mutation	BMC Med	9, Electronic resource # 69		2011年
Shibata M.A, Morimoto J, Shibata E, Harada-Shiba M, and Fujioka S	Inhibition of tumor growth and metastasis by a combination of anti-VEGF-C and enhanced IL-12 therapy in an immunocompetent mouse mammary cancer model	Breast Cancer - Current and Alternative Therapeutic Modalities		489-502	2011年

Biochimie 94 (2012) 1032–1040

Contents lists available at SciVerse ScienceDirect

Biochimie

journal homepage: www.elsevier.com/locate/biochi

Research paper

Chemical modification of triplex-forming oligonucleotide to promote pyrimidine motif triplex formation at physiological pH

Hidetaka Torigoe [a,*], Osamu Nakagawa [b], Takeshi Imanishi [b], Satoshi Obika [b], Kiyomi Sasaki [a]

[a] Department of Applied Chemistry, Faculty of Science, Tokyo University of Science, 1-3 Kagurazaka, Shinjuku-ku, Tokyo 162-8601, Japan
[b] Graduate School of Pharmaceutical Sciences, Osaka University, 1-6 Yamadaoka, Suita, Osaka 565-0871, Japan

ARTICLE INFO

Article history:
Received 21 June 2011
Accepted 4 January 2012
Available online 9 January 2012

Keywords:
Triplex formation
Chemical modification of triplex-forming oligonucleotide
Thermodynamic parameters
Rigidity
Hydration
Nuclease resistance

ABSTRACT

Extreme instability of pyrimidine motif triplex DNA at physiological pH severely limits its use in wide variety of potential applications, such as artificial regulation of gene expression, mapping of genomic DNA, and gene-targeted mutagenesis *in vivo*. Stabilization of pyrimidine motif triplex at physiological pH is, therefore, crucial for improving its potential in various triplex-formation-based strategies *in vivo*. To this end, we investigated the effect of 3′-amino-2′-*O*,4′-*C*-methylene bridged nucleic acid modification of triplex-forming oligonucleotide (TFO), in which 2′-O and 4′-C of the sugar moiety were bridged with the methylene chain and 3′-O was replaced by 3′-NH, on pyrimidine motif triplex formation at physiological pH. The modification not only significantly increased the thermal stability of the triplex but also increased the binding constant of triplex formation about 15-fold. The increased magnitude of the binding constant was not significantly changed when the number and position of the modification in TFO changed. The consideration of the observed thermodynamic parameters suggested that the increased rigidity of the modified TFO in the free state resulting from the bridging of different positions of the sugar moiety with an alkyl chain and the increased hydration of the modified TFO in the free state caused by the introduction of polar nitrogen atoms may significantly increase the binding constant at physiological pH. The study on the TFO viability in human serum showed that the modification significantly increased the resistance of TFO against nuclease degradation. This study presents an effective approach for designing novel chemically modified TFOs with higher binding affinity of triplex formation at physiological pH and higher nuclease resistance under physiological condition, which may eventually lead to progress in various triplex-formation-based strategies *in vivo*.

1. Introduction

In recent years, triplex nucleic acid has attracted considerable interest because of its possible biological functions *in vivo* and its wide variety of potential applications, such as artificial regulation of gene expression by antigene technology, mapping of genomic DNA, and gene-targeted mutagenesis [1–5]. A triplex nucleic acid is usually formed through the sequence-specific interaction of a single-stranded homopyrimidine or homopurine triplex-forming oligonucleotide (TFO) with the major groove of a homopurine–homopyrimidine stretch in duplex DNA [3,4]. In the pyrimidine motif triplex, a homopyrimidine TFO binds parallel to the homopurine strand of the target duplex by Hoogsteen hydrogen bonding to form T•A:T and C^+•G:C base triplets [3,4]. On the other hand, in the purine motif triplex, a homopurine TFO binds antiparallel to the homopurine strand of the target duplex by reverse Hoogsteen hydrogen bonding to form A•A:T (or T•A:T) and G•G:C base triplets [3,4].

Because protonation of the cytosine bases in a homopyrimidine TFO is required to enable binding with the guanine bases of the G:C target duplex, the formation of the pyrimidine motif triplex requires an environment with acidic pH, and is thus extremely unstable at physiological neutral pH [6–8]. On the other hand, the pH-independent formation of the purine motif triplex is possible at physiological neutral pH. However, purine motif triplex formation is severely inhibited by physiological concentrations of certain monovalent cations, especially K^+ ions [9,10]. The undefined association between K^+ and the guanine-rich homopurine TFO has been considered to explain this inhibitory effect [9,10]. Thus, the stabilization of the pyrimidine motif triplex at physiological neutral pH is necessary for improving its potential in various

Abbreviations: 3′-amino-2′,4′-BNA, 3′-amino-2′-*O*,4′-*C*-methylene bridged nucleic acid; CD, circular dichroism; EMSA, electrophoretic mobility shift assay; HPLC, high-performance liquid chromatography; ITC, isothermal titration calorimetry; TFO, triplex-forming oligonucleotide.

* Corresponding author. Tel.: +81 3 5228 8259; fax: +81 3 5261 4631.
E-mail address: htorigoe@rs.kagu.tus.ac.jp (H. Torigoe).

0300-9084/$ – see front matter © 2012 Elsevier Masson SAS. All rights reserved.
doi:10.1016/j.biochi.2012.01.003

triplex-formation-based strategies. Replacement of the cytosine bases in a homopyrimidine TFO with 5-methylcytosine [7,11–13] or other chemically modified base analogues [14–18], and conjugation of different DNA intercalators to TFO [19,20] have been used to overcome the requirement of an acidic pH for the pyrimidine motif triplex formation and to stabilize the pyrimidine motif triplex at physiological neutral pH.

We first synthesized and developed a new class of chemical modifications of nucleic acids, 3′-amino-2′-*O*,4′-*C*-methylene bridged nucleic acid (3′-amino-2′,4′-BNA) (Fig. 1a), in which 2′-O and 4′-C of the sugar moiety were bridged with the methylene chain, and 3′-O was replaced by 3′-NH [21,22]. The thermal stability of the triplex with 3′-amino-2′,4′-BNA modified TFO at physiological neutral pH was much higher than that with the corresponding natural phosphodiester TFO, which was shown by the UV melting of the dissociation of the triplex [21,22]. However, the formation of the triplex involving 3′-amino-2′,4′-BNA modified TFO at physiological neutral pH has not yet been well-characterized. To explore the possibility of the application of 3′-amino-2′,4′-BNA modified TFO to various triplex-formation-based strategies *in vivo*, the investigation of the formation of the triplex involving 3′-amino-2′,4′-BNA modified TFO at physiological neutral pH may be more important than that of the dissociation of the same triplex. In addition, the mechanistic explanation for the 3′-amino-2′,4′-BNA modification-mediated triplex stabilization at physiological neutral pH remains to be provided. Therefore, we have examined the effect of the 3′-amino-2′,4′-BNA modification of TFO on pyrimidine motif triplex formation with another base sequence at physiological neutral pH. The thermodynamic effect of the 3′-amino-2′,4′-BNA modification on the pyrimidine motif triplex formation between a 23-base pair homopurine-homopyrimidine target duplex (Pur23A•Pyr23T) (Fig. 1b) and its specific 15-mer unmodified homopyrimidine TFO (Pyr15T) (Fig. 1b) or each of 3′-amino-2′,4′-BNA modified homopyrimidine TFO (Pyr15BNANP7-1, Pyr15BNANP7-2, Pyr15BNANP5-1, and Pyr15BNANP5-2) (Fig. 1b) has been analyzed by the electrophoretic mobility shift assay (EMSA) [23–29], UV melting, and isothermal titration calorimetry (ITC) [24–26,28,30–33]. To examine the effect of the modified positions, Pyr15BNANP7-1 and Pyr15BNANP7-2 contain one modification every 2 nucleotides starting from the first and second positions at the 5′-terminal, respectively. Pyr15BNANP5-1 and Pyr15BNANP5-2 contain one modification every 3 nucleotides starting from the first and second positions at the 5′-terminal, respectively. To explore the possibility of the application of 3′-amino-2′,4′-BNA modified TFOs *in vivo*, the resistance of the unmodified and 3′-amino-2′,4′-BNA modified TFOs against nuclease degradation in human serum has been also investigated by native polyacrylamide gel electrophoresis and anion-exchange high-performance liquid chromatography (HPLC). We found that the 3′-amino-2′,4′-BNA modification of TFO increased the binding constant for the pyrimidine motif triplex formation at physiological neutral pH about 15-fold. We also observed that the nuclease resistance of the 3′-amino-2′,4′-BNA modified TFOs was significantly higher than that of the unmodified TFO. The mechanism of the 3′-amino-2′,4′-BNA modification to promote the pyrimidine motif triplex formation will be discussed. This information will present an effective approach for designing novel chemically modified TFOs with higher binding affinity of the pyrimidine motif triplex formation at physiological neutral pH.

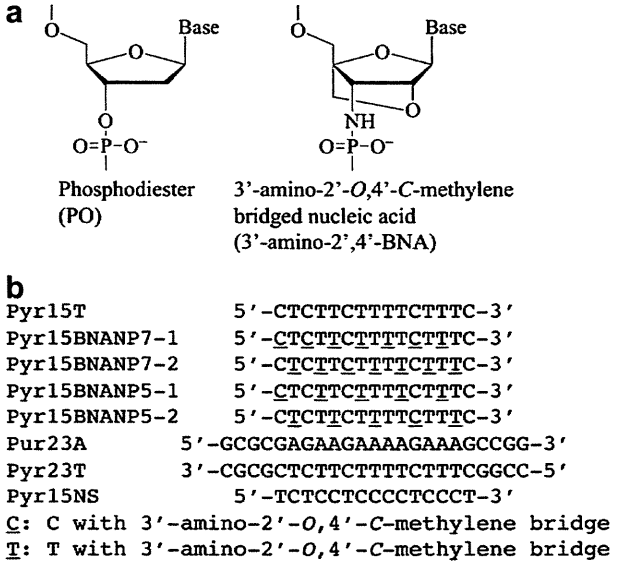

Fig. 1. (a) Structural formulas for phosphodiester (PO) and 3′-amino-2′-*O*,4′-*C*-methylene bridged nucleic acid (3′-amino-2′,4′-BNA)-modified backbones. (b) Oligonucleotide sequences for the target duplex (Pur23A•Pyr23T), the specific TFOs (Pyr15T, Pyr15BNANP7-1, Pyr15BNANP7-2, Pyr15BNANP5-1, and Pyr15BNANP5-2), and the nonspecific oligonucleotide (Pyr15NS).

2. Materials and methods

2.1. Preparation of oligonucleotides

We synthesized 23-mer complementary oligonucleotides for the target duplex, Pur23A and Pyr23T (Fig. 1b), a 15-mer unmodified homopyrimidine TFO specific to the target duplex, Pyr15T (Fig. 1b), and a 15-mer nonspecific homopyrimidine oligonucleotide, Pyr15NS (Fig. 1b), on an ABI DNA synthesizer using the solid-phase cyanoethyl phosphoramidite method; we then purified them by reverse-phase HPLC on a Wakosil DNA column. The 15-mer 3′-amino-2′,4′-BNA modified homopyrimidine TFOs specific to the target duplex, Pyr15BNANP7-1, Pyr15BNANP7-2, Pyr15BNANP5-1, and Pyr15BNANP5-2 (Fig. 1b), were synthesized and purified as described previously [21,22]. The concentration of all oligonucleotides was determined by UV absorbance. Complementary strands, Pur23A and Pyr23T, were annealed by heating up to 90 °C and then gradually cooling to room temperature. The annealed sample was applied to a hydroxyapatite column (BIORAD Inc.) to remove unpaired single strands. The concentration of the duplex DNA (Pur23A•Pyr23T) was determined by UV absorption, considering that an absorbance of 1 at 260 nm corresponds to a concentration of 50 μg/mL of DNA, with a M_r of 15180.

2.2. EMSA

EMSA experiments were performed as previously described, by 15% native polyacrylamide gel electrophoresis [24–29]. In a 9 μL aliquot of the reaction mixture, ^{32}P-labeled Pur23A•Pyr23T duplex (~1 nM) was mixed with increasing concentrations of the specific TFO (Pyr15T, Pyr15BNANP7-1, Pyr15BNANP7-2, Pyr15BNANP5-1, or Pyr15BNANP5-2) and the nonspecific oligonucleotide (Pyr15NS) in buffer [50 mM Tris-acetate (pH 7.0), 100 mM NaCl, and 10 mM $MgCl_2$]. Pyr15NS was added to achieve equimolar concentrations of TFO in each lane as well as to minimize the adhesion of the DNA (duplex and TFO) to plastic surfaces during incubation and subsequent losses during processing. After 6 h incubation at 37 °C, 2 μL of 50% glycerol solution containing bromophenol blue was added without changing the pH and salt concentrations of the reaction mixtures. Samples were then directly loaded onto a 15% native polyacrylamide gel prepared in buffer [50 mM Tris-acetate (pH 7.0) and 10 mM $MgCl_2$], and electrophoresis was performed at 8 V/cm for 16 h at 4 °C.

2.3. UV melting

UV melting experiments were carried out on a DU-640 spectrophotometer (Beckman Inc.) equipped with a Peltier-type cell holder. The cell path length was 1 cm. UV profiles were measured in buffer A (10 mM sodium cacodylate-cacodylic acid at pH 6.8 containing 200 mM NaCl and 20 mM $MgCl_2$) at a scan rate of 0.2 °C/min with detection at 260 nm for both melting and renaturing. The first derivative was calculated from the UV profiles. The peak temperature in the derivative curve was designated as the melting temperature, T_m. The triplex nucleic acid concentration used was 1 μM.

2.4. Circular dichroism (CD) spectroscopy

CD spectra at 20 °C were recorded in buffer A on a JASCO J-720 spectropolarimeter interfaced with a microcomputer. The cell path length was 1 cm. The triplex nucleic acid concentration used was 1 μM.

2.5. ITC

Isothermal titration experiments were carried out on a VP ITC system (Microcal Inc., U.S.A.) by following a previously described procedure [24–26,28]. The TFO and Pur23A•Pyr23T duplex solutions were prepared by extensive dialysis against buffer A or buffer B (10 mM sodium cacodylate-cacodylic acid at pH 5.8 containing 200 mM NaCl and 20 mM $MgCl_2$). The Pur23A•Pyr23T duplex solution in buffer A or buffer B was injected 20 times in 5 μL aliquots at 10 min intervals into the TFO solution without changing the reaction conditions. The heat of dilution of the injectant, which was measured by injecting the Pur23A•Pyr23T duplex solution into the same buffer, was subtracted from the heat of each injection. Each corrected heat value was divided by the number of moles of the Pur23A•Pyr23T duplex solution injected, and analyzed with Microcal Origin software supplied by the manufacturer.

2.6. Viability of TFO in human serum

Viability of TFO in human serum was examined by the following two procedures.

2.6.1. Analyses by native polyacrylamide gel electrophoresis

TFO was 5′-end labeled with ^{32}P using [γ-^{32}P] ATP and T4 polynucleotide kinase by using a standard procedure. An amount of 2 pmol of ^{32}P-labeled TFO was incubated at 37 °C in 200 μL of human serum from human male AB plasma (Sigma–Aldrich Co., USA). Aliquots of 5 μL were removed after 10, 20, 40, 60, and 120 min of incubation and mixed with 5 μL of stop solution (80% formamide, 50 mM EDTA) to terminate the reaction. The samples were loaded on 15% native polyacrylamide gels prepared in buffer [50 mM Tris-acetate (pH 7.0) and 100 mM $MgCl_2$], and electrophoresis was performed at 8 V/cm and 4 °C. The gels were scanned and analyzed by using a BAS system.

2.6.2. Analyses by anion-exchange HPLC

An amount of 1 nmol of TFO was incubated at 37 °C in 20 μL of 50% human serum from human male AB plasma (Sigma–Aldrich Co., USA). After incubation for 20, 60, and 120 min, each sample was mixed with 13 μL of formamide to terminate the reaction, and the samples were stored at −80 °C until HPLC analysis. The samples were mixed with 400 μL of HPLC buffer [25 mM Tris–HCl (pH 7.0) and 0.5% CH_3CN] and analyzed by anion-exchange HPLC on JASCO LC-2000 Plus series with detection at 260 nm by using a linear gradient of 0–0.5 M NH_4Cl in HPLC buffer over 45 min to resolve the products. The HPLC column used was TSK-GEL DNA-NPR (Tosoh, Japan). Under these conditions, peaks of all proteins from the human serum could be distinguished from those of the intact and degraded TFO. Degradation data from the acquired chromatograms were processed using ChromNAV software supplied by the manufacturer.

3. Results

3.1. Electrophoretic mobility shift assay of pyrimidine motif triplex formation at physiological neutral pH

The pyrimidine motif triplex formation of the target duplex (Pur23A•Pyr23T; Fig. 1b) with its specific unmodified (Pyr15T; Fig. 1b) or 3′-amino-2′,4′-BNA modified (Pyr15BNANP7-1, Pyr15BNANP7-2, Pyr15BNANP5-1, or Pyr15BNANP5-2; Fig. 1b) TFO was examined at pH 7.0 by EMSA (Fig. 2). Total oligonucleotide concentration ([specific TFO (Pyr15T, Pyr15BNANP7-1, Pyr15BNANP7-2, Pyr15BNANP5-1, or Pyr15BNANP5-2; Fig. 1b)] + [nonspecific oligonucleotide (Pyr15NS; Fig. 1b)]) was kept constant at 1 μM to minimize loss of DNA during processing and to assess sequence specificity. While incubation with 1 μM Pyr15NS alone did not cause a shift in the electrophoretic migration of the target duplex (see *lane 1* for Pyr15T), those with Pyr15T, Pyr15BNANP7-1, Pyr15BNANP7-2, Pyr15BNANP5-1, or Pyr15BNANP5-2 at particular concentrations caused retardation of the

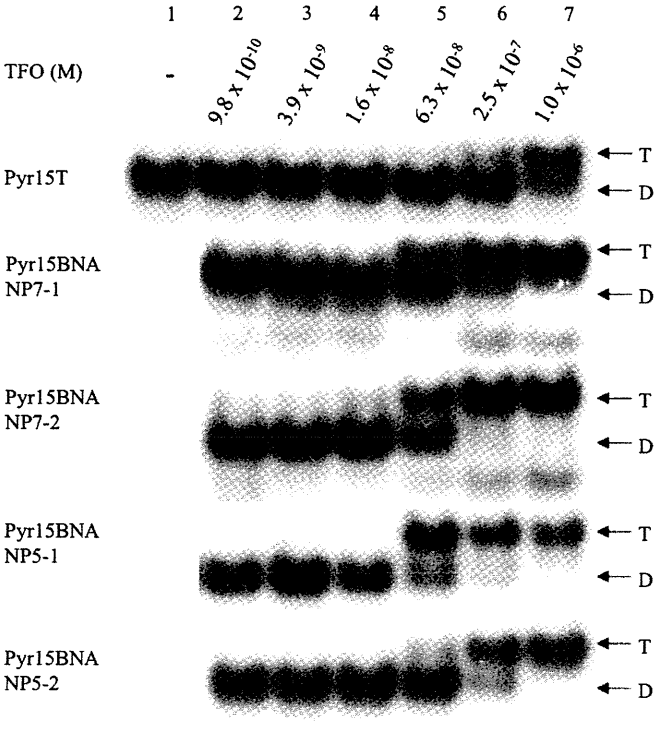

Fig. 2. EMSA of pyrimidine motif triplex formation using specific TFOs (Pyr15T, Pyr15BNANP7-1, Pyr15BNANP7-2, Pyr15BNANP5-1, or Pyr15BNANP5-2) at physiological neutral pH. Triplex formation was initiated by adding ^{32}P-labeled Pur23A•Pyr23T duplex (~1 nM) with the indicated final concentrations of the specific TFOs (Pyr15T, Pyr15BNANP7-1, Pyr15BNANP7-2, Pyr15BNANP5-1, or Pyr15BNANP5-2). The nonspecific oligonucleotide (Pyr15NS) was added to adjust to equimolar concentration (1 μM) of TFO (Pyr15T+Pyr15NS, Pyr15BNANP7-1+Pyr15NS, Pyr15BNANP7-2+Pyr15NS, Pyr15BNANP5-1+Pyr15NS, or Pyr15BNANP5-2+Pyr15NS) in each lane. Reaction mixtures involving Pyr15T, Pyr15BNANP7-1, Pyr15BNANP7-2, Pyr15BNANP5-1, or Pyr15BNANP5-2 in 50 mM Tris-acetate (pH 7.0), 100 mM NaCl, and 10 mM $MgCl_2$ were incubated for 6 h at 37 °C, and then electrophoretically separated at 4 °C on a 15% native polyacrylamide gel prepared in buffer [50 mM Tris-acetate (pH 7.0) and 10 mM $MgCl_2$]. Positions of the duplex (D) and triplex (T) are indicated.

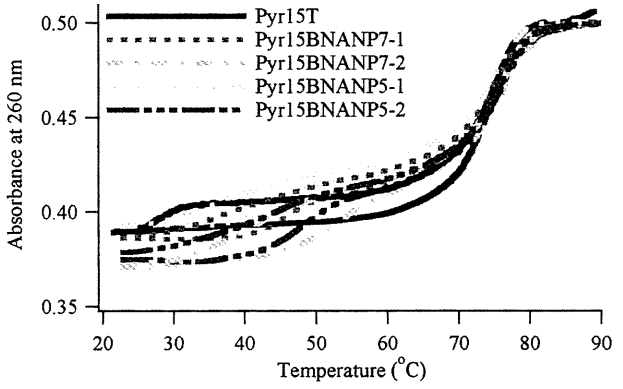

Fig. 3. UV profiles of pyrimidine motif triplexes formed with specific TFOs (Pyr15T, Pyr15BNANP7-1, Pyr15BNANP7-2, Pyr15BNANP5-1, or Pyr15BNANP5-2) for both melting and renaturing. The triplexes with Pyr15T, Pyr15BNANP7-1, Pyr15BNANP7-2, Pyr15BNANP5-1, or Pyr15BNANP5-2 in 10 mM sodium cacodylate-cacodylic acid (pH 6.8), 200 mM NaCl and 20 mM $MgCl_2$ were melted and renatured at a scan rate of 0.2 °C/min with detection at 260 nm. The cell path length was 1 cm. The triplex nucleic acid concentration used was 1 μM.

duplex migration owing to triplex formation [23]. The dissociation constant, K_d, of triplex formation was determined from the concentration of the TFO, which caused half of the target duplex to shift to the triplex [23]. K_d of the triplex with Pyr15T was estimated to be ~1 μM. In contrast, K_d of the triplex with each of the modified TFOs, Pyr15BNANP7-1, Pyr15BNANP7-2, Pyr15BNANP5-1, and Pyr15BNANP5-2 was ~0.06 μM, indicating that the 3′-amino-2′,4′-BNA modification of TFO increased the binding constant, K_a (= 1/K_d), of pyrimidine motif triplex formation at physiological neutral pH about 16-fold. The increase in K_a due to the modification was similar in magnitude among the four modified TFOs.

3.2. Spectroscopic characterization of pyrimidine motif triplex at physiological neutral pH

The thermal stability of the pyrimidine motif triplex with the unmodified or 3′-amino-2′,4′-BNA modified TFOs was investigated at pH 6.8 by UV profile for both melting and renaturing (Fig. 3 and Table 1). All the triplexes showed two-step transitions. The first transition at the lower temperature, T_{m1}, corresponded to the transition of the triplex to a duplex and a TFO, and the second transition at the higher temperature, T_{m2}, corresponded to the transition of the duplex to two single-strands (Fig. 3). The T_{m2} values were almost identical among all the triplexes (Table 1). Although a kind of irreversibility was observed for all TFOs [34], the T_{m1} values for the association and dissociation of Pyr15BNANP7-1, Pyr15BNANP7-2, Pyr15BNANP5-1, or Pyr15BNANP5-2 with the target duplex were significantly larger than that of Pyr15T in both the melting and renaturing curves (Table 1). These results demonstrate that the thermal stability of the triplexes with 3′-amino-2′,4′-BNA modified TFO was significantly higher than that with the unmodified TFO, confirming our previous result [21,22] that the 3′-amino-2′,4′-BNA modification of TFO increased the thermal stability of the pyrimidine motif triplex at physiological neutral pH. In addition, we examined the temperature dependence of the absorbance at 295 nm for the triplexes involving unmodified or 3′-amino-2′,4′-BNA modified TFOs to follow the deprotonation and protonation of the cytosines in triplex denaturation and formation (Figure S1 in Supplementary Material) [35]. Although the change of the absorbance at 295 nm during temperature shift was significantly smaller than that at 260 nm, the temperature range of deprotonation and protonation of the cytosines for Pyr15BNANP7-1, Pyr15BNANP7-2, Pyr15BNANP5-1, or Pyr15BNANP5-2 was higher than that for Pyr15T in spite of a kind of irreversibility for all TFOs (Figure S1 in Supplementary Material).

Table 1
Melting temperatures of the triplexes between a 23-base pair target duplex (Pur23A•Pyr23T) and a 15-mer TFO (Pyr15T, Pyr15BNANP7-1, Pyr15BNANP7-2, Pyr15BNANP5-1, or Pyr15BNANP5-2) in 10 mM sodium cacodylate-cacodylic acid (pH 6.8), 200 mM NaCl and 20 mM $MgCl_2$ for both melting and renaturing.

TFO	T_{m1} (°C) melting	T_{m1} (°C) renaturing	T_{m2} (°C) melting	T_{m2} (°C) renaturing
Pyr15T	28.5 ± 0.2	23.1 ± 0.5	73.5 ± 0.1	72.9 ± 0.3
Pyr15BNANP7-1	53.3 ± 0.1	45.3 ± 0.2	73.5 ± 0.1	73.4 ± 0.1
Pyr15BNANP7-2	53.3 ± 0.1	44.7 ± 0.1	73.5 ± 0.3	73.9 ± 0.1
Pyr15BNANP5-1	50.3 ± 0.1	45.7 ± 0.1	73.5 ± 0.2	73.3 ± 0.3
Pyr15BNANP5-2	52.2 ± 0.5	45.2 ± 0.1	72.9 ± 0.3	73.9 ± 0.2

To further characterize the triplexes involving the unmodified or 3′-amino-2′,4′-BNA modified TFOs, CD spectra of the triplexes were measured at 20 °C and pH 6.8 (Fig. 4). The overall shape of the CD spectra was similar among all the profiles. A significant negative band in the short-wavelength (210–220 nm) region was observed in all the profiles, confirming triplex formation involving each TFO [36]. The intensity of the negative short-wavelength (210–220 nm) band for the triplexes involving each of the modified TFOs, Pyr15BNANP7-1, Pyr15BNANP7-2, Pyr15BNANP5-1, and Pyr15BNANP5-2 was larger than that observed for the triplex involving Pyr15T, indicating that all the triplexes involving the 3′-amino-2′,4′-BNA modified TFO had more features of the A-like conformation than that involving the unmodified TFO [37].

3.3. Thermodynamic analyses of pyrimidine motif triplex formation by ITC

We examined the thermodynamic parameters of the pyrimidine motif triplex formation between a 23-base pair target duplex (Pur23A•Pyr23T) and its specific 15-mer unmodified (Pyr15T) or 3′-amino-2′,4′-BNA modified (Pyr15BNANP7-1, Pyr15BNANP7-2, Pyr15BNANP5-1, or Pyr15BNANP5-2) TFO at 25 °C and pH 6.8 by ITC. To investigate the pH dependence of the pyrimidine motif triplex formation, the thermodynamic parameters of the triplex formation between Pur23A•Pyr23T and Pyr15T were also analyzed at 25 °C and pH 5.8 by ITC. Fig. 5a shows a typical ITC profile for the triplex formation between Pyr15BNANP7-1 and Pur23A•Pyr23T at

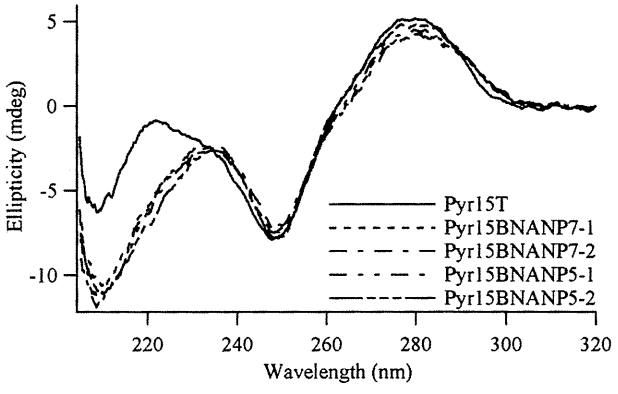

Fig. 4. CD spectra of pyrimidine motif triplexes formed with specific TFOs (Pyr15T, Pyr15BNANP7-1, Pyr15BNANP7-2, Pyr15BNANP5-1, or Pyr15BNANP5-2). The triplexes with Pyr15T, Pyr15BNANP7-1, Pyr15BNANP7-2, Pyr15BNANP5-1, or Pyr15BNANP5-2 in 10 mM sodium cacodylate-cacodylic acid (pH 6.8), 200 mM NaCl and 20 mM $MgCl_2$ were measured at 20 °C in the wavelength range of 205–320 nm. The cell path length was 1 cm. The triplex nucleic acid concentration used was 1 μM.

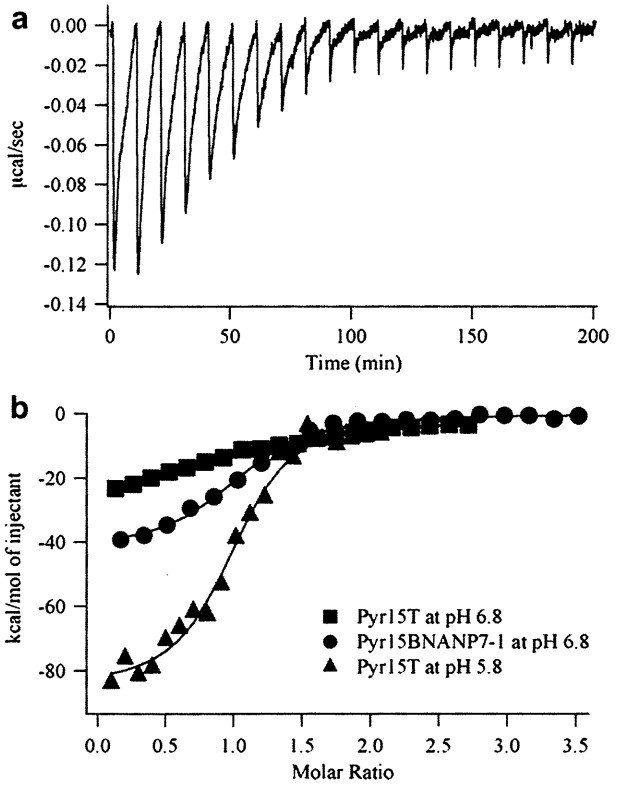

Fig. 5. Thermodynamic analyses of pyrimidine motif triplex formation using Pyr15T or Pyr15BNANP7-1 at pH 6.8, and Pyr15T at pH 5.8 by ITC. (a) Typical ITC profiles for the triplex formation between Pyr15BNANP7-1 and Pur23A•Pyr23T at 25 °C and pH 6.8. Pur23A•Pyr23T solution (140 μM) in 10 mM sodium cacodylate-cacodylic acid (pH 6.8), 200 mM NaCl and 20 mM $MgCl_2$ was injected 20 times in 5 μL aliquots into 3.0 μM Pyr15BNANP7-1 solution, which was dialyzed against the same buffer. Aliquots were injected over 12 s at 10 min intervals. (b) Titration plots as a function of the molar ratio [Pur23A•Pyr23T]/[TFO]. The data were fitted by a nonlinear least-squares method.

25 °C and pH 6.8. An exothermic heat pulse was observed after each injection of Pur23A•Pyr23T into Pyr15BNANP7-1. The magnitude of each peak decreased gradually with each new injection, and a small peak was still observed at the molar ratio corresponding to the last injection. The area of the small peak was equal to the heat of dilution measured in a separate experiment by injecting Pur23A•Pyr23T into the same buffer. The area under each peak was integrated, and the heat of dilution of Pur23A•Pyr23T was subtracted from the integrated values. The corrected heat value was divided by the moles of injected solution, and the resulting values were plotted as a function of the molar ratio of [Pur23A•Pyr23T]/[Pyr15BNANP7-1], as shown in Fig. 5b. A sigmoidal curve was fitted to the resultant titration plot by a nonlinear least-squares method. The binding constant, K_a, and the enthalpy change, ΔH, were obtained from the fitted curve [32]. The Gibbs free energy change, ΔG, and the entropy change, ΔS, were calculated from the equation, $\Delta G = -RT\ln K_a = \Delta H - T\Delta S$, where R is the gas constant and T is the temperature [32]. The titration plots for Pyr15T at pH 6.8 and pH 5.8 are also shown in Fig. 5b. The thermodynamic parameters for Pyr15T at pH 6.8 and pH 5.8 were obtained from the titration plots in the same way. The ITC profiles and the titration plots for Pyr15BNANP7-2, Pyr15BNANP5-1, and Pyr15BNANP5-2 at pH 6.8 were almost the same as those observed for Pyr15BNANP7-1 at pH 6.8. The thermodynamic parameters for Pyr15BNANP7-2, Pyr15BNANP5-1, and Pyr15BNANP5-2 at pH 6.8 were obtained from the titration plots in the same way.

Table 2 summarizes the thermodynamic parameters for the formation of pyrimidine motif triplexes with Pyr15T, Pyr15BNANP7-1, Pyr15BNANP7-2, Pyr15BNANP5-1, and Pyr15BNANP5-2 at 25 °C and pH 6.8 and for the formation with Pyr15T at 25 °C and pH 5.8, obtained from ITC. The signs of both ΔH and ΔS were negative under each condition. Because an observed negative ΔS was unfavorable for triplex formation, triplex formation was driven by a large negative ΔH under each condition. K_a for Pyr15T at pH 5.8 was about 20-fold larger than that observed for Pyr15T at pH 6.8, confirming, like others [6–8], that physiological neutral pH is unfavorable for the pyrimidine motif triplex formation involving C^+•G:C triads. In addition, K_a for each of the 3′-amino-2′,4′-BNA modified TFOs at pH 6.8 was about 15-fold larger than that observed for Pyr15T at pH 6.8, indicating that the 3′-amino-2′,4′-BNA modification of TFO increased K_a for the pyrimidine motif triplex formation at physiological neutral pH, which is consistent with the results of EMSA (Fig. 2). The increase in K_a due to TFO modification was similar in magnitude among the four modified TFOs. Further, although the K_a and ΔG values for triplex formation with each of the modified TFOs at pH 6.8 and with Pyr15T at pH 5.8 were quite similar, the components of ΔG, that is, ΔH and ΔS, obviously differed in value (Table 2). The absolute values of the negative ΔH and ΔS for each of the modified TFOs at pH 6.8 were significantly smaller than those observed for Pyr15T at pH 5.8 (Table 2).

To examine the significance of 3′-amino modification in the 3′-amino-2′,4′-BNA modification, we investigated thermodynamic parameters for the triplex formation involving 2′,4′-BNA modified TFOs at pH 6.8 by ITC (Table S1 in Supplementary Material). The positions of 2′,4′-BNA modification were the same as those of 3′-amino-2′,4′-BNA modification. K_a for 2′,4′-BNA modified TFOs at pH 6.8 was about 4-fold larger than that observed for Pyr15T at pH 6.8 (Table S1 in Supplementary Material). On the other hand, K_a for 3′-amino-2′,4′-BNA modified TFOs at pH 6.8 was about 15-fold larger than that observed for Pyr15T at pH 6.8 (Table 2). Thus, K_a at pH 6.8 promoted by 2′,4′-BNA modification was significantly further increased by 3′-amino modification. 3′-amino modification significantly contributes to enhancement of the pyrimidine motif triplex formation at physiological neutral pH.

To examine the generality of the effect of 3′-amino-2′,4′-BNA modification to promote pyrimidine motif triplex formation at physiological neutral pH, we investigated thermodynamic

Table 2
Thermodynamic parameters for the triplex formation between a 23-base pair target duplex (Pur23A•Pyr23T) and a 15-mer TFO (Pyr15T, Pyr15BNANP7-1, Pyr15BNANP7-2, Pyr15BNANP5-1, or Pyr15BNANP5-2) at 25 °C, obtained from ITC.

TFO	pH	K_a (M^{-1})	K_a (relative)	ΔG (kcal mol^{-1})	ΔH (kcal mol^{-1})	ΔS (cal mol^{-1} K^{-1})
Pyr15T	5.8[a]	$(3.83 \pm 0.74) \times 10^6$	19.4	−8.98 ± 0.13	−85.6 ± 2.6	−257 ± 9.1
Pyr15T	6.8[b]	$(1.97 \pm 0.43) \times 10^5$	1.0	−7.22 ± 0.15	−34.9 ± 2.2	−92.7 ± 8.0
Pyr15BNANP7-1	6.8[b]	$(2.43 \pm 0.39) \times 10^6$	12.3	−8.71 ± 0.10	−48.3 ± 2.0	−133 ± 6.9
Pyr15BNANP7-2	6.8[b]	$(2.52 \pm 0.51) \times 10^6$	12.8	−8.73 ± 0.14	−56.4 ± 3.3	−160 ± 11.4
Pyr15BNANP5-1	6.8[b]	$(2.43 \pm 0.18) \times 10^6$	12.3	−8.71 ± 0.05	−48.3 ± 3.1	−133 ± 10.6
Pyr15BNANP5-2	6.8[b]	$(2.98 \pm 0.48) \times 10^6$	15.1	−8.83 ± 0.10	−53.2 ± 2.6	−149 ± 9.0

[a] 10 mM sodium cacodylate-cacodylic acid (pH 5.8), 200 mM NaCl and 20 mM $MgCl_2$.
[b] 10 mM sodium cacodylate-cacodylic acid (pH 6.8), 200 mM NaCl and 20 mM $MgCl_2$.

parameters for the triplex formation with another base sequence between 21-bp target duplex and each of 15-mer unmodified or 3′-amino-2′,4′-BNA modified TFO (Table S2 in Supplementary Material). Only one 3′-amino-2′,4′-BNA modification was introduced just in the middle of 15-mer TFO. K_a for the 3′-amino-2′,4′-BNA modified TFO at pH 7.0 was significantly larger than that observed for the unmodified TFO at pH 7.0, indicating that even only one 3′-amino-2′,4′-BNA modification of TFO increased K_a for the pyrimidine motif triplex formation at physiological neutral pH, which is consistent with the results of Table 2.

3.4. Viability of TFOs in human serum against nuclease degradation

A major difficulty associated with the use of oligonucleotides as *in vivo* agents is their rapid degradation by nuclease *in vivo* [38]. To explore the possibility of the use of 3′-amino-2′,4′-BNA modified TFOs in various triplex-formation-based strategies *in vivo*, we examined the resistance of the unmodified or 3′-amino-2′,4′-BNA modified TFOs to nuclease degradation. The series of TFOs 5′-end labeled with ^{32}P were incubated at 37 °C in human serum, and their degradation was assessed by 15% native polyacrylamide gel electrophoresis (Figure S2 in Supplementary Material). The entire Pyr15T was degraded and converted to shorter oligonucleotides within 10 min of incubation. In contrast, most of Pyr15BNANP7-2 and Pyr15BNANP5-2 remained intact even after 120 min of incubation. These results indicate that the 3′-amino-2′,4′-BNA modification contributed to an increase in the viability of TFOs in human serum. Because Pyr15BNANP7-1 and Pyr15BNANP5-1 containing the 3′-amino-2′,4′-BNA modification at the 5′-end could not be labeled with ^{32}P by T4 polynucleotide kinase, it was impossible to examine the resistance of Pyr15BNANP7-1 and Pyr15BNANP5-1 in human serum. Thus, to investigate the resistance of all TFOs, including Pyr15BNANP7-1 and Pyr15BNANP5-1, against nuclease degradation, their degradation was estimated by anion-exchange HPLC after incubating the TFOs at 37 °C in human serum. Fig. 6 shows the percentage of intact oligonucleotides as a function of the incubation time. Only 20% of intact Pyr15T was detected after 20 min of incubation with human serum, and Pyr15T was completely degraded within 60 min. On the other hand, more than 50% of each of the 3′-amino-2′,4′-BNA modified TFOs remained intact even after 120 min of incubation with human serum. These results indicate that the 3′-amino-2′,4′-BNA modification significantly increased the nuclease resistance of TFOs in human serum. The results of anion-exchange HPLC are consistent with those of native polyacrylamide gel electrophoresis (Figure S2 in Supplementary Material).

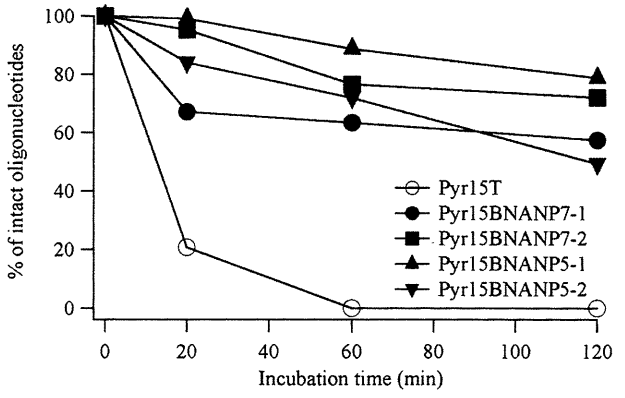

Fig. 6. Viability of specific TFOs (Pyr15T, Pyr15BNANP7-1, Pyr15BNANP7-2, Pyr15BNANP5-1, and Pyr15BNANP5-2) in human serum. TFOs (1 nmol) were incubated in human serum at 37 °C, and aliquots were removed at the time points indicated and analyzed by anion-exchange HPLC. The percentage of intact oligonucleotides was determined and plotted as a function of the incubation time.

4. Discussion

K_a of the pyrimidine motif triplex formation with Pyr15T at pH 5.8 was about 20-fold larger than that observed with Pyr15T at pH 6.8 (Table 2), which is consistent with the previously reported results that physiological neutral pH is unfavorable for pyrimidine motif triplex formation involving $C^+ \cdot G{:}C$ triads [6–8]. On the other hand, K_a of the pyrimidine motif triplex formation with each of the 3′-amino-2′,4′-BNA modified TFOs at pH 6.8 was about 15-fold larger than that observed with Pyr15T at pH 6.8 (Table 2). The increase in K_a at physiological neutral pH by the modification of TFO was supported by the results of EMSA (Fig. 2). Although the magnitudes of K_d ($=1/K_a$) were different between EMSA (Fig. 2) and ITC (Table 2) due to the difference in the experimental buffer conditions, the modification of TFO promoted the pyrimidine motif triplex formation in both buffer conditions. In addition, the modification of TFO increased the thermal stability of the pyrimidine motif triplexes at physiological neutral pH (Fig. 3 and Table 1), which confirmed our previous results [21,22]. These results indicate that the 3′-amino-2′,4′-BNA modification of TFO promotes the pyrimidine motif triplex formation at physiological neutral pH. The 3′-amino-2′,4′-BNA modification of TFO may promote the assembly of the 3′-amino-2′,4′-BNA modified TFO and the target duplex, which may enhance protonation of cytosine bases of the 3′-amino-2′,4′-BNA modified TFO to form the triplex. The pK_a increase of cytosine bases of the 3′-amino-2′,4′-BNA modified TFO in the triplex may be caused by the intrinsic stability of the triplex involving the 3′-amino-2′,4′-BNA modified TFO.

Because the formed triplex structures involving Pyr15T at pH 5.8 and Pyr15T at pH 6.8 are the same, the absolute values of ΔH and ΔS involved in the triplex formation measured by ITC could in fact be the same for the two conditions. However, the absolute values of ΔH and ΔS for Pyr15T at pH 6.8 were significantly smaller than those observed for Pyr15T at pH 5.8. When ΔH and ΔS are calculated from the fitting procedure of ITC, the value of the heat observed by ITC is divided not by the effective concentration really involved in the triplex formation, but by the apparent concentration added to the triplex formation [32]. The calculation does not take into consideration what percentage of the added concentration is actually effectively involved in the triplex formation. Thus, if the triplex formation is substoichiometric under a certain condition, the absolute values of ΔH and ΔS estimated by ITC are smaller than those observed for the more stoichiometric triplex formation under another condition. Therefore, the significantly smaller absolute values of ΔH and ΔS for Pyr15T at pH 6.8 relative to those for Pyr15T at pH 5.8 (Table 2) suggest that the triplex formation with Pyr15T at pH 6.8 was significantly more substoichiometric than that with Pyr15T at pH 5.8. This was also supported by the significantly smaller absolute values of K_a and ΔG for Pyr15T at pH 6.8 (Table 2). In contrast, the K_a and ΔG values for Pyr15T at pH 5.8 and those for the 3′-amino-2′,4′-BNA modified TFOs at pH 6.8 were quite similar (Table 2), suggesting that the triplex formations under these conditions were similarly quite stoichiometric. We conclude that the triplex formation with Pyr15T at pH 6.8 was significantly more substoichiometric than that with Pyr15T at pH 5.8 and that with the 3′-amino-2′,4′-BNA modified TFOs at pH 6.8. Thus, to discuss the mechanism for promotion of triplex formation by 3′-amino-2′,4′-BNA modification of TFO, the comparison between the values of ΔH and ΔS observed for Pyr15T at pH 6.8 and those for the modified TFOs at pH 6.8 is not valid due to the significantly lower stoichiometry for Pyr15T at pH 6.8. The comparison between the values of ΔH and ΔS for Pyr15T at pH 5.8 and those for modified TFOs at pH

6.8 with similar stoichiometry will indicate a reasonable mechanism for the promotion of triplex formation by the modification of TFO, as discussed below.

Although the values of K_a and ΔG for Pyr15T at pH 5.8 and those for the 3′-amino-2′,4′-BNA modified TFOs at pH 6.8 were quite similar (Table 2), the components of ΔG, that is, ΔH and ΔS, were obviously different in value. The absolute values of the negative ΔH and ΔS for the modified TFOs at pH 6.8 were smaller than those observed for Pyr15T at pH 5.8 (Table 2). The observed negative ΔH upon triplex formation, measured by ITC, reflects a major contribution from the hydrogen bonding and the base stacking involved in triplex formation [39–42]. The immobilization of electrostricted water molecules around polar atoms upon triplex formation is also considered to be a major contributor to the observed negative ΔH of triplex formation [39–42]. The value of ΔH also includes a contribution from the protonation of cytosine bases upon hydrogen bonding, and the accompanying deprotonation of the cacodylate buffer releasing protons to bind with the cytosine bases [43]. Because the degree of protonation may be similar between the modified TFOs at pH 6.8 and Pyr15T at pH 5.8 because of the similarity of stoichiometry discussed above, and as the protons that bind with the cytosine bases are released from the same cacodylate buffer in both cases, the values of ΔH derived from the protonation of the cytosine bases and the accompanying deprotonation of the cacodylate buffer should be similar in the two cases. Thus, the difference in ΔH of formation between the stoichiometric triplexes with modified TFOs at pH 6.8 and Pyr15T at pH 5.8 (Table 2) suggests that the hydrogen bonding and/or the base stacking in the triplexes with modified TFO and the degree of immobilization of water molecules around the protonated cytosine bases and polar nitrogen atoms of the triplexes with the modified TFO may be significantly different from that with the corresponding unmodified TFO. In fact, the CD spectra show that the triplexes with 3′-amino-2′,4′-BNA modified TFO had more features of the A-like conformation than that with the corresponding unmodified TFO (Fig. 4) [37]. The A-like conformation obtained by the modification of TFO may result in the difference in the negative ΔH between the unmodified and modified TFOs. On the other hand, contributions to ΔS observed upon triplex formation measured by ITC mainly come from two factors: a negative conformational entropy change from the conformational restraint of the TFO involved in triplex formation and a positive dehydration entropy change resulting from the release of structured water molecules surrounding the TFO and the target duplex upon triplex formation [39–42]. Therefore, one of the reasons for the smaller magnitude of the negative ΔS for the 3′-amino-2′,4′-BNA modified TFOs at pH 6.8 in comparison with that for Pyr15T at pH 5.8 (Table 2) may be a result of the negative conformational entropy change. The 3′-amino-2′,4′-BNA modified TFO in the free state may be more rigid than the corresponding unmodified TFO, because the 2′-O and 4′-C positions of the sugar moiety of the 3′-amino-2′,4′-BNA are bridged with a methylene chain. The increased rigidity of the modified TFO in the free state relative to the corresponding unmodified TFO may lead to a smaller loss of conformational entropy upon triplex formation in the case of the modified TFO at physiological neutral pH. Another reason for the smaller magnitudes of the negative ΔS for the 3′-amino-2′,4′-BNA modified TFOs at pH 6.8 relative to that for Pyr15T at pH 5.8 (Table 2) may be inferred from the positive dehydration entropy change. Previous studies on crystallographic structures [44] and molecular dynamics simulation [45,46] showed that the degree of hydration around the N3′-phosphoramidate backbone was enhanced in comparison with that around the corresponding DNA phosphodiester backbone. The increased hydration of the modified TFO in the free state relative to the corresponding unmodified TFO may cause a larger gain of dehydration entropy upon triplex formation with the modified TFO at physiological neutral pH. These two possible reasons, the smaller loss of conformational entropy and the larger gain of dehydration entropy, may account for the smaller magnitudes of the negative ΔS observed for the modified TFOs at pH 6.8. This provides a favorable component to ΔG and leads to the increase in K_a of triplex formation at physiological neutral pH. In conclusion, because the smaller absolute values of the negative ΔH for the modified TFOs at pH 6.8 in comparison with that for Pyr15T at pH 5.8 were unfavorable for promotion of triplex formation (Table 2), the hydrogen bonding and the base stacking, which are major contributions to the observed ΔH upon triplex formation, cannot be major factors contributing to promote the pyrimidine motif triplex formation at physiological neutral pH. On the other hand, because the smaller absolute values of the negative ΔS for the modified TFOs at pH 6.8 in comparison with that for Pyr15T at pH 5.8 were favorable for promotion of triplex formation (Table 2), the increased rigidity and the increased hydration of the modified TFO in the free state, which are major contributions to the observed ΔS upon triplex formation, are major factors contributing to the increase in K_a of the pyrimidine motif triplex formation at physiological neutral pH.

The increase in K_a by the 3′-amino-2′,4′-BNA modification was similar in magnitude among the four modified TFOs (Fig. 2 and Table 2), indicating that the number and position of the modification did not significantly affect the magnitude of increase in K_a at physiological neutral pH. The increased rigidity and hydration of the modified TFO may be more important than the variation of the number and position of the modification in achieving the increase in K_a of the pyrimidine motif triplex formation at physiological neutral pH. Thus, other modification strategies to achieve increased rigidity and hydration of TFO may also be useful to increase K_a of the pyrimidine motif triplex formation at physiological neutral pH.

The nuclease resistance of 3′-amino-2′,4′-BNA modified TFO was significantly higher than that of the unmodified TFO (Fig. 6 and Figure S2 in Supplementary Material). The modification increased the nuclease resistance of TFOs in human serum. Previously, the nuclease resistance of the phosphorothioate backbone, in which a nonbridging oxygen of a phosphodiester group was replaced by a sulfur atom, was known to be significantly higher than that of the unmodified backbone [47,48]. However, K_a of triplex formation with the phosphorothioate modified TFO was significantly smaller than that with the unmodified TFO [33,49]. Thus, the phosphorothioate modification increased the nuclease resistance of TFO, but it decreased the triplex forming ability. On the other hand, as discussed above, the 3′-amino-2′,4′-BNA modification of TFO increased the pyrimidine motif triplex forming ability at physiological neutral pH (Fig. 2 and Table 2). Therefore, the 3′-amino-2′,4′-BNA modification enhanced both the nuclease resistance of TFO and the pyrimidine motif triplex forming ability at physiological neutral pH. We conclude that due to these excellent properties 3′-amino-2′,4′-BNA modification may be more favorable than phosphorothioate modification upon application of TFO to various pyrimidine motif triplex-formation-based strategies *in vivo*.

5. Conclusions

The present study has clearly demonstrated that the 3′-amino-2′,4′-BNA modification of TFO promoted pyrimidine motif triplex formation at physiological neutral pH. It has also shown that the modification of TFO increased the nuclease resistance of TFO in human serum. Our results certainly support the idea that the 3′-amino-2′,4′-BNA modified oligonucleotides may have the potential to be applied to various pyrimidine motif triplex-formation-based strategies, such as artificial regulation of gene expression by antigene technology, mapping of genomic DNA, and gene-targeted

mutagenesis. In addition, the present study has shown that the increased rigidity and the increased hydration of the modified TFO in the free state may enable the significant increase in K_a for the pyrimidine motif triplex formation at physiological neutral pH. We conclude that the design of TFO, involving the bridging of different positions of the sugar moiety with an alkyl chain for increased rigidity and the introduction of polar nitrogen atoms for increased hydration, is certainly promising for the promotion of pyrimidine motif triplex formation at physiological neutral pH, which may eventually lead to progress in various pyrimidine motif triplex-formation-based strategies.

Acknowledgments

This work was supported in part by a Grant-in-Aid for Scientific Research on Innovative Areas (22113519 to H.T.), Grant-in-Aid for Exploratory Research (20655038 to S. O.), Grant-in-Aid for Scientific Research (B) (21350094 to S.O.), and Grant-in-Aid for JSPS Fellows (22-10383 to K.S.) from the Ministry of Education, Science, Sports, and Culture of Japan. This work was also supported partly by the Program for Promotion of Fundamental Studies in Health Sciences of the National Institute of Biomedical Innovation (NIBIO).

Appendix. Supplementary data

Supplementary data associated with this article can be found, in the online version, at doi:10.1016/j.biochi.2012.01.003.

References

[1] J.Y. Chin, E.B. Schleifman, P.M. Glazer, Repair and recombination induced by triple helix DNA, Front. Biosci. 12 (2007) 4288–4297.
[2] J.J. Bissler, Triplex DNA and human disease, Front. Biosci. 12 (2007) 4536–4546.
[3] M. Duca, P. Vekhoff, K. Oussedik, L. Halby, P.B. Arimondo, The triple helix: 50 years later, the outcome, Nucleic Acids Res. 36 (2008) 5123–5138.
[4] A. Jain, G. Wang, K.M. Vasquez, DNA triple helices: biological consequences and therapeutic potential, Biochimie 90 (2008) 1117–1130.
[5] R.D. Wells, DNA triplexes and Friedreich ataxia, Faseb J. 22 (2008) 1625–1634.
[6] M.D. Frank-Kamenetskii, Protonated DNA structures, Methods Enzymol. 211 (1992) 180–191.
[7] S.F. Singleton, P.B. Dervan, Influence of pH on the equilibrium association constants for oligodeoxyribonucleotide-directed triple helix formation at single DNA sites, Biochemistry 31 (1992) 10995–11003.
[8] H. Shindo, H. Torigoe, A. Sarai, Thermodynamic and kinetic studies of DNA triplex formation of an oligohomopyrimidine and a matched duplex by filter binding assay, Biochemistry 32 (1993) 8963–8969.
[9] J.F. Milligan, S.H. Krawczyk, S. Wadwani, M.D. Matteucci, An anti-parallel triple helix motif with oligodeoxynucleotides containing 2'-deoxyguanosine and 7-deaza-2'-deoxyxanthosine, Nucleic Acids Res. 21 (1993) 327–333.
[10] A.J. Cheng, M.W. Van Dyke, Monovalent cation effects on intermolecular purine-purine-pyrimidine triple-helix formation, Nucleic Acids Res. 21 (1993) 5630–5635.
[11] J.S. Lee, M.L. Woodsworth, L.J. Latimer, A.R. Morgan, Poly(pyrimidine). poly(-purine) synthetic DNAs containing 5-methylcytosine form stable triplexes at neutral pH, Nucleic Acids Res. 12 (1984) 6603–6614.
[12] T.J. Povsic, P.B. Dervan, Triple helix formation by oligonucleotides on DNA Extended to the physiological Ph range, J. Am. Chem. Soc. 111 (1989) 3059–3061.
[13] L.E. Xodo, G. Manzini, F. Quadrifoglio, G.A. van der Marel, J.H. van Boom, Effect of 5-methylcytosine on the stability of triple-stranded DNA–a thermodynamic study, Nucleic Acids Res. 19 (1991) 5625–5631.
[14] A. Ono, P.O.P. Tso, L.S. Kan, Triplex formation of oligonucleotides containing 2'-O-Methylpseudoisocytidine in Substitution for 2'-Deoxycytidine, J. Am. Chem. Soc. 113 (1991) 4032–4033.
[15] S.H. Krawczyk, J.F. Milligan, S. Wadwani, C. Moulds, B.C. Froehler, M.D. Matteucci, Oligonucleotide-mediated triple helix formation using an N3-protonated deoxycytidine analog exhibiting pH-independent binding within the physiological range, Proc. Natl. Acad. Sci. U S A 89 (1992) 3761–3764.
[16] J.S. Koh, P.B. Dervan, Design of a Nonnatural Deoxyribonucleoside for Recognition of Gc base-pairs by oligonucleotide-directed triple helix formation, J. Am. Chem. Soc. 114 (1992) 1470–1478.
[17] M.C. Jetter, F.W. Hobbs, 7,8-Dihydro-8-oxoadenine as a replacement for cytosine in the third strand of triple helices. Triplex formation without hypochromicity, Biochemistry 32 (1993) 3249–3254.
[18] Y. Ueno, M. Mikawa, A. Matsuda, Nucleosides and nucleotides. 170. Synthesis and properties of oligodeoxynucleotides containing 5-[N-[2-[N, N-bis(2-aminoethyl)- amino]ethyl]carbamoyl]-2'-deoxyuridine and 5-[N-[3-[N, N-bis(3-aminopropyl) amino]propyl]carbamoyl]-2'-deoxyuridine, Bioconjug. Chem. 9 (1998) 33–39.
[19] J.S. Sun, C. Giovannangeli, J.C. Francois, R. Kurfurst, T. Montenay-Garestier, U. Asseline, T. Saison-Behmoaras, N.T. Thuong, C. Helene, Triple-helix formation by alpha oligodeoxynucleotides and alpha oligodeoxynucleotide-intercalator conjugates, Proc. Natl. Acad. Sci. U S A 88 (1991) 6023–6027.
[20] J.F. Mouscadet, C. Ketterle, H. Goulaouic, S. Carteau, F. Subra, M. Le Bret, C. Auclair, Triple helix formation with short oligonucleotide-intercalator conjugates matching the HIV-1 U3 LTR end sequence, Biochemistry 33 (1994) 4187–4196.
[21] S. Obika, M. Onoda, K. Morita, J. Andoh, M. Koizumi, T. Imanishi, 3'-amino-2',4'-BNA: novel bridged nucleic acids having an N3'–>P5' phosphoramidate linkage, Chem. Commun. (Camb) (2001) 1992–1993.
[22] S. Obika, S.M. Rahman, B. Song, M. Onoda, M. Koizumi, K. Morita, T. Imanishi, Synthesis and properties of 3'-amino-2',4'-BNA, a bridged nucleic acid with a N3'–>P5' phosphoramidate linkage, Bioorg. Med. Chem. 16 (2008) 9230–9237.
[23] V.I. Lyamichev, S.M. Mirkin, M.D. Frank-Kamenetskii, C.R. Cantor, A stable complex between homopyrimidine oligomers and the homologous regions of duplex DNAs, Nucleic Acids Res. 16 (1988) 2165–2178.
[24] H. Torigoe, A. Ferdous, H. Watanabe, T. Akaike, A. Maruyama, Poly(L-lysine)-graft-dextran copolymer promotes pyrimidine motif triplex DNA formation at physiological pH – thermodynamic and kinetic studies, J. Biol. Chem. 274 (1999) 6161–6167.
[25] H. Torigoe, Y. Hari, M. Sekiguchi, S. Obika, T. Imanishi, 2'-O,4'-C-methylene bridged nucleic acid modification promotes pyrimidine motif triplex DNA formation at physiological pH: thermodynamic and kinetic studies, J. Biol. Chem. 276 (2001) 2354–2360.
[26] H. Torigoe, Thermodynamic and kinetic effects of N3'–>P5' phosphoramidate modification on pyrimidine motif triplex DNA formation, Biochemistry 40 (2001) 1063–1069.
[27] H. Torigoe, A. Maruyama, Synergistic stabilization of nucleic acid assembly by oligo-N3'–>P5' phosphoramidate modification and additions of comb-type cationic copolymers, J. Am. Chem. Soc. 127 (2005) 1705–1710.
[28] H. Torigoe, K. Sasaki, T. Katayama, Thermodynamic and kinetic effects of morpholino modification on pyrimidine motif triplex nucleic acid formation under physiological condition, J. Biochem. 146 (2009) 173–183.
[29] H. Torigoe, A. Maruyama, S. Obika, T. Imanishi, T. Katayama, Synergistic stabilization of nucleic acid assembly by 2'-O,4'-C-methylene-bridged nucleic acid modification and additions of comb-type cationic copolymers, Biochemistry 48 (2009) 3545–3553.
[30] N. Langerman, R.L. Biltonen, Microcalorimeters for biological chemistry: applications, instrumentation and experimental design, Methods Enzymol. 61 (1979) 261–286.
[31] R.L. Biltonen, N. Langerman, Microcalorimetry for biological chemistry: experimental design, data analysis, and interpretation, Methods Enzymol. 61 (1979) 287–318.
[32] T. Wiseman, S. Williston, J.F. Brandts, L.N. Lin, Rapid measurement of binding constants and heats of binding using a new titration calorimeter, Anal. Biochem. 179 (1989) 131–137.
[33] H. Torigoe, R. Shimizume, A. Sarai, H. Shindo, Triplex formation of chemically modified homopyrimidine oligonucleotides: thermodynamic and kinetic studies, Biochemistry 38 (1999) 14653–14659.
[34] M. Rougee, B. Faucon, J.L. Mergny, F. Barcelo, C. Giovannangeli, T. Garestier, C. Helene, Kinetics and thermodynamics of triple-helix formation: effects of ionic strength and mismatches, Biochemistry 31 (1992) 9269–9278.
[35] L. Lavelle, J.R. Fresco, UV spectroscopic identification and thermodynamic analysis of protonated third strand deoxycytidine residues at neutrality in the triplex $d(C(+)\text{-}T)_6$:$[d(A\text{-}G)_6.d(C\text{-}T)_6]$; evidence for a proton switch, Nucleic Acids Res. 23 (1995) 2692–2705.
[36] G. Manzini, L.E. Xodo, D. Gasparotto, F. Quadrifoglio, G.A. van der Marel, J.H. van Boom, Triple helix formation by oligopurine-oligopyrimidine DNA fragments. Electrophoretic and thermodynamic behavior, J. Mol. Biol. 213 (1990) 833–843.
[37] K.H. Johnson, D.M. Gray, J.C. Sutherland, Vacuum UV CD spectra of homopolymer duplexes and triplexes containing A.T or A.U base pairs, Nucleic Acids Res. 19 (1991) 2275–2280.
[38] E. Wickstrom, Oligodeoxynucleotide stability in subcellular extracts and culture media, J. Biochem. Biophys. Methods 13 (1986) 97–102.
[39] H. Edelhoch, J.C. Osborne Jr., The thermodynamic basis of the stability of proteins, nucleic acids, and membranes, Adv. Protein Chem. 30 (1976) 183–250.
[40] Y.K. Cheng, B.M. Pettitt, Stabilities of double- and triple-strand helical nucleic acids, Prog. Biophys. Mol. Biol. 58 (1992) 225–257.
[41] M. Kamiya, H. Torigoe, H. Shindo, A. Sarai, Temperature dependence and sequence specificity of DNA triplex formation: an analysis using isothermal titration calorimetry, J. Am. Chem. Soc. 118 (1996) 4532–4538.
[42] R.H. Shafer, Stability and structure of model DNA triplexes and quadruplexes and their interactions with small ligands, Prog. Nucleic Acid Res. Mol. Biol. 59 (1998) 55–94.
[43] H. Fukada, K. Takahashi, Enthalpy and heat capacity changes for the proton dissociation of various buffer components in 0.1M potassium chloride, Proteins 33 (1998) 159–166.
[44] V. Tereshko, S. Gryaznov, M. Egli, Consequences of replacing the DNA 3'-oxygen by an amino group: high-resolution crystal structure of a fully